


Research Article

Myosin Va interacts with the exosomal protein spermine synthase

Luciano G. Dolce^{1,2,*}, Rui M. P. Silva-Junior^{4,*}, Leandro H. P. Assis^{1,2}, Andrey F. Z. Nascimento^{1,5}, Jackeline S. Araujo⁴, Ingrid P. Meschede⁴, Enilza M. Espreafico⁴, Priscila O. de Giuseppe^{2,3} and  Mário T. Murakami^{2,3}

¹Graduate Program in Functional and Molecular Biology, Institute of Biology, University of Campinas, Campinas, São Paulo, Brazil; ²Brazilian Biosciences National Laboratory (LNBio), Brazilian Center for Research in Energy and Materials (CNPEM), Zip Code 13083-970, Campinas, São Paulo, Brazil; ³Brazilian Bioethanol Science and Technology Laboratory (CTBE), Brazilian Center for Research in Energy and Materials (CNPEM), Zip code 13083-970, Campinas, São Paulo, Brazil; ⁴Department of Cell and Molecular Biology, Faculty of Medicine of Ribeirão Preto, University of São Paulo, Ribeirão Preto, São Paulo, Brazil; ⁵Brazilian Synchrotron Light Laboratory (LNLS), Brazilian Center for Research in Energy and Materials (CNPEM), Campinas, Zip code 13083-970, São Paulo, Brazil

Correspondence: Mario Tyago Murakami (mario.murakami@ctbe.cnpem.br) or Priscila Oliveira de Giuseppe (priscila.giuseppe@ctbe.cnpem.br) or Enilza Maria Espreafico (emespre@fmrp.usp.br)



Myosin Va (MyoVa) is an actin-based molecular motor that plays key roles in the final stages of secretory pathways, including neurotransmitter release. Several studies have addressed how MyoVa coordinates the trafficking of secretory vesicles, but why this molecular motor is found in exosomes is still unclear. In this work, using a yeast two-hybrid screening system, we identified the direct interaction between the globular tail domain (GTD) of MyoVa and four protein components of exosomes: the WD repeat-containing protein 48 (WDR48), the cold shock domain-containing protein E1 (CSDE1), the tandem C2 domain-containing protein 1 (TC2N), and the enzyme spermine synthase (SMS). The interaction between the GTD of MyoVa and SMS was further validated *in vitro* and displayed a K_d in the low micromolar range ($3.5 \pm 0.5 \mu\text{M}$). SMS localized together with MyoVa in cytoplasmic vesicles of breast cancer MCF-7 and neuroblastoma SH-SY5Y cell lines, known to produce exosomes. Moreover, *MYO5A* knockdown decreased the expression of *SMS* gene and rendered the distribution of SMS protein diffuse, supporting a role for MyoVa in SMS expression and targeting.

Introduction

Class V myosins are processive motors that transport or tether vesicles, organelles, and macromolecules to actin filaments, and play key roles in synaptic transmission, hormone secretion, and plasma membrane homeostasis [1–6]. They can be divided into four major structural domains with specific functions: the motor domain, which contains the actin-binding site and displays ATPase activity, the lever arm that provides a large powerstroke to occur after ATP hydrolysis, the rod region, responsible for dimerization, and the globular tail domain (GTD), a protein-binding module that allows multiple roles for these molecular motors [3,4,7–10]. In humans, three paralogous genes encode for class V myosins: *MYO5A*, *MYO5B*, and *MYO5C*. Defects in the *MYO5A* gene are related to the Griscelli syndrome type 1 (also known as Elejalde syndrome) [11,12], which is characterized by partial albinism and severe neurological disorders. The molecular mechanism behind the partial albinism involves defects on a tripartite complex between myosin Va (MyoVa), melanophilin, and Rab27a for melanosomes transport [13,14]. However, for the pleiotropic effects of *MYO5A* mutation in neurodevelopment, the mechanisms are still poorly understood [15].

In neuronal cells, MyoVa has been associated with organelle transport, mRNA trafficking and exocytosis of secretory vesicles [1,2]. Particularly in exocytosis, MyoVa seems to play several roles, including the capture and transport of the secretory granules in the F-actin-rich cortex, the remodeling of their

* These authors contributed equally to this work.

Received: 26 November 2018

Revised: 31 January 2019

Accepted: 05 February 2019

Accepted Manuscript Online: 07 February 2019

Version of Record published: 01 March 2019

membranes required for maturation, and their controlled release [16]. To date, most of the studies about MyoVa have focused on understanding how it regulates the trafficking of secretory vesicles. However, none of them have investigated whether MyoVa could also influence the internal composition of such vesicles, even though MyoVa is recurrently found in extracellular vesicles called exosomes [17].

In this work, to investigate whether MyoVa directly interacts with soluble protein components of exosomes, we performed a two-hybrid screening using the GTD of MyoVa as bait and a universal human-normalized library as prey. As envisaged, we identified the interaction of MyoVa-GTD with four proteins that compose exosomes, including the enzyme spermine synthase (SMS), which plays key roles in neurodevelopment and brain function. SMS interacts with MyoVa-GTD *in vitro*, with a K_d in the low micromolar range, and localizes together with MyoVa in vesicles at the cytoplasm of two exosome-producer cell types. *MYO5A* gene silencing led to a diffuse distribution of SMS, indicating a novel role of MyoVa in the targeting of this enzyme to secretory vesicles. Moreover, either *MYO5A* knockdown or knockout decreased *SMS* gene expression, supporting that MyoVa may influence the synthesis or stability of *SMS* mRNA. As SMS produces the neuromodulator spermine, which is stored in secretory vesicles and released via exocytosis, our findings might have implications not only in the targeting of spermine synthase to exosomes but also in the molecular mechanisms underlying the secretion of spermine.

Materials and methods

Yeast two-hybrid screening

The yeast two-hybrid screening was performed using the Matchmaker[®] Gold yeast two-hybrid system (Takara Bio – Clontech) according to the manufacturer's instructions. All reagents used in this screen was purchased from Takara Bio – Clontech, unless stated otherwise. The MyoVa-GTD-S1651E/S1652E [9] coding sequence (residues 1448–1855; NP_000250.3) was subcloned into the *EcoRI* and *SalI* sites of pGBKT7 (pGBKT7-EE construct), and was used to transform *Saccharomyces cerevisiae* Y2H Gold[®] strain. This phosphomimetic (EE) construct was the bait because our original aim was to identify phospho-specific interactions. The pGADT7-Prey plasmid of clones positive for the activation of all reporter genes of the system (*HIS3*, *ADE2*, *AUR1-C*, and *MEL1*) were extracted using the Easy Yeast Plasmid Isolation Kit. The purified vectors were transformed into *Escherichia coli* DH5 α competent cells, extracted with the QIAprep Spin Miniprep Kit (Qiagen), submitted to DNA sequencing, and compared with non-redundant sequence databases using BLASTn and BLASTx [18].

Yeast two-hybrid pairwise validation

To validate the positive hits identified in the yeast two-hybrid screen and to test whether the interactions were dependent of the phosphomimetic mutation, *S. cerevisiae* Y2H Gold[®] cells were co-transformed with a pair of pGBKT7 and pGADT7 vectors (Supplementary Table S1), and grown at 30°C for 4 days on QDO/X/A-agar plates – a synthetic defined agar medium without tryptophan, leucine, histidine and adenine, and supplemented with 200 ng/ml aureobasidin A and 40 μ g/ml 5-bromo-4-chloro-3-indolyl alpha-D-galactopyranoside (Takara Bio – Clontech). To remove potential false-positive results, we tested the activation of all reporter genes in Y2H Gold[®] cells co-transformed with pGADT7-Prey and empty pGBKT7 vectors (negative controls).

Bioinformatics validation

The nucleotide sequences of preys validated in the previous step were subjected to bioinformatics analyses to filter out possible false positives still present. Initially, the sequences were analyzed using BLASTn [18] to remove those hits containing 5' or 3' UTR in frame with the GAL4 AD sequence, which would generate artificial fusion proteins. For constructs containing truncated open reading frames (ORF), only those hits containing at least one intact domain were considered as true positives, according to protein sequence analyses using the SMART server [19].

Molecular cloning

The full-length *SMS* ORF (NM_004595.4, 253-1353 pb) was amplified from a human cDNA library by PCR using the primers shown in Supplementary Table S2. The PCR product was purified with QIAquick PCR Purification Kit (Qiagen), digested using *NdeI* and *XhoI* restriction enzymes and inserted into the *NdeI/XhoI* sites of pET28a tobacco etch virus (TEV) vector [9] using T4 DNA Ligase (Promega). Positive clones were confirmed by DNA sequencing.

Microscale thermophoresis

To perform the microscale thermophoresis (MST) experiment, the wild-type MyoVa-GTD [9] and *SMS* constructs (both in pET28a-TEV vector) were produced in BL21(DE3) Δ SlyD strain containing the plasmid pRARE2, in LB

medium [20] at 25°C for 4 h, and 20°C for 16 h, respectively. The cell lysis was performed by sonication (Vibra-cells, Sonics) with lysis buffer (50 mM HEPES, 500 mM NaCl, 5% (v/v) glycerol, 20 mM imidazole, pH 7.4) supplemented with 0.1 mg/ml lysozyme, and SIGMAFAST™ Protease Inhibitor Tablets (Sigma-Aldrich). All proteins were purified by two chromatographic steps, using a HiTrap Chelating column (GE Healthcare), with an imidazole gradient for protein elution, and a HiLoad Superdex 200 (or 75) 16/60 column (GE Healthcare). The size-exclusion chromatography (SEC) was carried out in SEC buffer (20 mM HEPES, 150 mM NaCl, 5% (v/v) glycerol, pH 7.4). MyoVa-GTD purified by affinity chromatography was treated with a His-tagged TEV protease [21] (4°C, 20 h) for the cleavage of the 6xHis-tag before the purification in a HiLoad Superdex 200 16/60 column (GE Healthcare) pre-equilibrated with SEC buffer.

The MST experiment was performed using a Monolith™ NT.115 (NanoTemper Technologies) device, with a LED power of 40%, and a MST power of 60%. SMS was labeled with the His-Tag Labeling Kit RED-tris-NTA (NanoTemper Technologies), following the manufacturer's labeling protocol, and loaded into Monolith™ NT.115 MST premium-coated capillaries (NanoTemper Technologies). All assays were performed in triplicate using 50 nM His-tagged-labeled-SMS and a serial dilution of MyoVa-GTD to the maximum possible concentration in SEC buffer. The differences between the cold and hot states of each of the 16 MST profiles were used to determine the change in fluorescence intensities for each profile using the following equation: $F_{norm} = F_{hot}/F_{cold} \cdot 1000$, where F is the fluorescence measured in each state. The data were processed using the NTAffinity Analysis software (NanoTemper Technologies) and the mean of F_{norm} triplicates plotted against ligand concentration were fitted with the Hill equation ($F_{norm} = [L]^n / K_d + [L]^n$, where [L] = ligand concentration, n = Hill coefficient, and K_d = dissociation constant) using the Origin 8.0 software to estimate the K_d .

Immunocytochemistry and gene silencing assays

Immunocytochemistry assays were performed on human neuroblastoma (SH-SY5Y) and human mammary adenocarcinoma (MCF-7) cell lines cultured in Dulbecco's modified Eagle's medium (DMEM) with high glucose (GIBCO - Thermo Fisher Scientific: 12800-017) supplemented with 10% (v/v) fetal bovine serum (FBS) 100 units/ml penicillin and 100 µg/ml of streptomycin and kept in a humid atmosphere containing 5% (v/v) CO₂ at 37°C. The Stealth RNAi™ siRNAs targeting *MYO5A* were purchased from Invitrogen - Thermo Fisher Scientific and are shown in Supplementary Table S3. A scramble sequence Stealth RNAi™ siRNA Negative Control High GC Duplex (Invitrogen - Thermo Fisher Scientific) was used as a control.

MCF-7 cells were transfected using DharmaFECT 1 Transfection Reagent (GE Healthcare) according to the manufacturer's instructions. Cells were fixed with 2% (v/v) paraformaldehyde pH 7.4 for 20 min, and then permeabilized with 0.3% (v/v) Triton X-100, blocked with 100 mM glycine, and then 3% (m/v) BSA (adapted from Assis et al. [7]). The following antibodies were used: 1 µg/ml rabbit anti-SMS (Sigma-Aldrich: HPA029852); 2 µg/ml rat polyclonal affinity-purified anti-MyoVa_Medial_Tail (*in house*, manuscript in preparation). Secondary antibodies used were 2 µg/ml Alexa Fluor® goat anti-rat 488 (Abcam: ab150157), 2 µg/ml Alexa Fluor® donkey anti-rabbit 594 (Molecular Probes: A21207) IgG. The slides were mounted on ProLong® Diamond Antifade Mountant medium with DAPI (Thermo Fisher Scientific: P36962) and the images were collected on Zeiss LSM780 Axio Observer multifotons inverted confocal microscope, with a 63× objective. The Icy BioImage open source software from the Pasteur Institute (<http://icy.bioimageanalysis.org/>) was used for image processing and calculation of the Pearson's coefficients with the colocalization studio plugin [22]. All the compared images were acquired with the same parameters. The raw files were used for all quantifications.

RNA isolation and quantitative PCR

Total RNA was extracted from the cells samples according to standard TRIzol protocol (Invitrogen - Thermo Fisher Scientific). Total RNA (1 µg) was reverse transcribed to cDNA using High Capacity cDNA Reverse Transcription Kit (Applied Biosystems - Thermo Fisher Scientific) according to a standard manufacturer's protocol followed by amplification on the ABI 7500 Real-Time PCR System (Applied Biosystems - Thermo Fisher Scientific), using primers from the Supplementary Table S4. Samples of SH-SY5Y cells (control and differentiated) were prepared as described below. All quantitative PCR (qPCR) analyses were performed in triplicate. The expression of endogenous control (GAPDH) was used for the normalization of RNA input.

Gene expression levels were calculated by relative quantitation using the ABI 7500 Real-Time PCR SDS 1.2 software (Applied Biosystems - Thermo Fisher Scientific) and the fold expression changes were determined by $2^{-\Delta\Delta C_T}$ method [23]. The data are presented as the fold change of mRNA expression in cells treated with siRNA relative to cells treated

with siControl after normalization to an endogenous control (GAPDH or TBP). The qPCR data were described as mean \pm standard deviation and analyzed using the Student's *t* test, with $P \leq 0.01$ considered statistically significant.

Neuronal differentiation

SH-SY5Y cells were cultivated in DMEM high glucose (GIBCO – Thermo Fisher Scientific: 12800-017), supplemented with 10% (v/v) FBS (GIBCO – Thermo Fisher Scientific) and 100 units/ml penicillin and 100 μ g/ml of streptomycin (GIBCO – Thermo Fisher Scientific: 15140122) and kept in a humid atmosphere containing 5% (v/v) CO₂ at 37°C. Cellular differentiation was induced as described by Encinas and coworkers [24] with some modifications. Briefly, 2.5×10^4 cells/cm² were plated on DMEM high glucose medium supplemented with 10% (v/v) FBS and 1% penicillin/streptomycin solution, in culture plates or on 13 mm² glass coverslips previously treated with 0.1 mg/ml poly-D-lysine (Sigma-Aldrich). The next day, the medium was removed and replaced with medium II (DMEM high glucose medium containing 1% (v/v) FBS, 1% penicillin/streptomycin solution and 10 μ M retinoic acid [Abcam: ab120728]). After 3 days of growth, medium was replaced with fresh medium II supplemented with 50 ng/ml brain-derived neurotrophic factor (BDNF; Sigma-Aldrich: SRP3014) and cells were grown for further 4 days. RNA extraction and qPCR assays were performed as described above.

Culture of FO and RO fibroblasts

FO cells are human fibroblasts isolated from skin fragments of a patient carrying a mutation in the *MYO5A* gene, which renders these cells null for MyoVa protein (Griscelli Syndrome type I/Elejalde syndrome). RO cells are normal human fibroblasts age-paired with FO, also isolated in the same laboratory, and used as control. The cells were cultured in DMEM high glucose (GIBCO – Thermo Fisher Scientific: 12800-017) supplemented with 10% (v/v) FBS (GIBCO – Thermo Fisher Scientific), at 37°C, 5% (v/v) CO₂. Total RNA was extracted using standard TRIzol protocol and used for cDNA synthesis and qPCR, as described above. All methods presented here were performed in accordance with the relevant guidelines and regulations approved by Faculty of Medicine of Ribeirão Preto, University of São Paulo and in accordance with The Code of Ethics of the World Medical Association (Declaration of Helsinki). Primary cultures were established with the informed consent of the patients and with the approval of the Research Ethics Committee of the Faculty of Medicine of Ribeirão Preto.

Results

Using MyoVa-GTD as bait, we obtained 54 clones in a yeast two-hybrid screen of a human-normalized cDNA library. These clones represented 35 different genes, according to DNA sequence analyses of the prey plasmids. To further validate these results, we performed a pairwise two-hybrid assay resulting in 21 positive clones. However, nine of them were from noncoding regions, such as 5' and 3' UTRs of mRNA, and three encoded zinc finger proteins or heat shock proteins, which are recurrent false positives in yeast two-hybrid assays [25] (Table 1). After the exclusion of truncated single-domain proteins (probably misfolded), four clones remained as potential binding partners of MyoVa-GTD: SMS, WDR48, CSDE1, and TC2N (Figure 1A,B). Interestingly, these four proteins are known components of exosomes (Table 2). Further, we evaluated whether these interactions could be regulated by the MyoVa-GTD phosphorylation at Ser1652. However, the four proteins interacted with both the GTD-EE (S1651E/S1652E) and GTD-AA (S1651A/S1652A) constructs in a pairwise two-hybrid assay, indicating that their binding to GTD is independent of the phosphorylation under the tested conditions (Figure 1A). The Ala mutant was used to mimic the nonphosphorylated state of MyoVa-GTD and preserves the structure and dynamic behavior of the wild-type construct produced in *E. coli* [9].

After analyzing the functional data available for SMS, WDR48, CSDE1, and TC2N in the literature, we decided to further characterize the interaction between MyoVa-GTD and SMS due to the key role of this enzyme in neurodevelopment [26,27]. For *in vitro* affinity assays, MyoVa-GTD and SMS proteins were expressed and purified to homogeneity (Supplementary Figures S1 and S2), the His-tag of MyoVa-GTD was removed, and the purified SMS protein was labeled with the RED-tris-NTA dye (Supplementary Figure S3). According to MST experiments, MyoVa-GTD and SMS formed a complex *in vitro* with a dissociation constant of $3.5 \pm 0.5 \mu$ M (Figure 1C), supporting SMS as a novel MyoVa-binding partner.

In breast cancer (MCF-7) and neuroblastoma (SH-SY5Y) cell lines, SMS localized together with a subset of MyoVa-labeled vesicles at the cytoplasm (Figure 2). We also noticed that *MYO5A* knockdown induced a more diffuse distribution of SMS, in contrast to the fewer, but sharper puncta observed at the control (Figure 3A), indicating that MyoVa may play a role in the targeting of SMS to vesicles.

Table 1 Positive results of pairwise yeast two-hybrid assays curated by bioinformatic analyses

Clone	Blastn result	Prey interval aligned to the mRNA (pb)	mRNA translation interval (pb)	Prey interval aligned to the polypeptide (aa)	Protein name (Length)	Domain composition (Position)	Description
2	NM_005180.8	1084–2167	507–1487				ZnF – Recurrent false positive
4	XM_011519161.1	88–1216	4739–7036				5' UTR
6	NM_001306191.1	793–1779	242–637				3' UTR
7	NM_006016.4	1549–1724	182–775				3' UTR
16	BC050683.1	302–1241	451–1887				ZnF – Recurrent false positive
19	NM_018442.3	2122–2736	354–2996	589–794*	<i>DDB1 and CUL4 associated factor 6</i> (880)	Several WD40 repeat domains	Probably misfolded protein
25	AC002549.1	92606–91778					Chromosomal untranscribed regions
30	NM_020839.3	1395–2380	41–2074	451–677	WD repeat-containing protein 48 (677)	WD40 (20–390) e DUF 3337 (509–674)	Regulator of deubiquitinating complexes [42]
36	AL049695.20	39457–40568					Chromosomal untranscribed regions
44	BC016058.1	810–1785	230–1219	193–329	<i>Cathepsin K</i> (329)	I29 (26–86) e Pept_C1 (105–320)	Probably misfolded protein
49	BC000006.2	584–1255	122–1033	154–303	<i>ATPase, Na⁺/K⁺ transporting, beta 1 polypeptide</i> (303)	Na ₂ K-ATPase (3–297)	Probably misfolded protein
68	NM_001165979.2	7561–7955	635–7495				3' UTR
78	NG_008805.2	8745–9860	396–9011	2783–2871	<i>Fibrillin 1</i> (2871)		Unfolded region
88	NR_033192.1	198–1074	45–774				HSP – Recurrent false positive
104	BC038384.1	894–1513	121–1095	258–324	<i>Y box binding protein 1</i> (324)	CSP (60–128)	Unfolded region
106	NM_138773.2	3372–4495	127–1383				3' UTR
108	AL139288.15	138495–139600					Chromosomal untranscribed regions
123	NG_009228.1	293–831	23–1129	90–269 *	Spermine synthase (366)	Spermine synth (89–366)	Converts spermidine into spermine [32]
142	NM_152332.5	1045–2180	214–1686	277–490	Tandem C2 domains nuclear protein (490)	C2 (240–340) e C2 (375–480)	Synaptotagmin-like tandem C2 protein
151	XM_006716253.2	4257–5384	115–972				3' UTR
186	NM_001007553.2	2590–3749	514–2910	692–798	Cold shock domain-containing protein E1 (798)	CSP (26–89), CSP (190–250), CSP (350–420), CSP (520–590), CSP (675–740) e SUZ-C (750–790)	RNA-binding protein [43]

Potential MyoVa-binding partners are highlighted in bold.

*The final pb identified in our sequencing, not the final pb in the prey.

Table 2 Proteins that interacted with MyoVa-GTD in the yeast two-hybrid system are components of exosomes and/or secretory vesicles

Protein	Tissue/cell type [vesicle type]	Database [ID]	Ref.
SMS	Breast cancer cells [exosomes]	Vesiclepedia [VP_20603]	[44]
WDR48	Breast cancer cells [exosomes]; melanoma cells [extracellular vesicles]; Mouse embryonic fibroblasts [extracellular vesicles]	Vesiclepedia [VP_67561]	[44]
TC2N	Breast milk [exosomes]; colorectal cancer cells [microvesicles]; Mesenchymal stem cells [microvesicles]; urine [exosomes]	Vesiclepedia [VP_123036]	[44]
CSDE1	Mast cells [exosomes]	Exocarta [ExoCarta_229663]	[17]

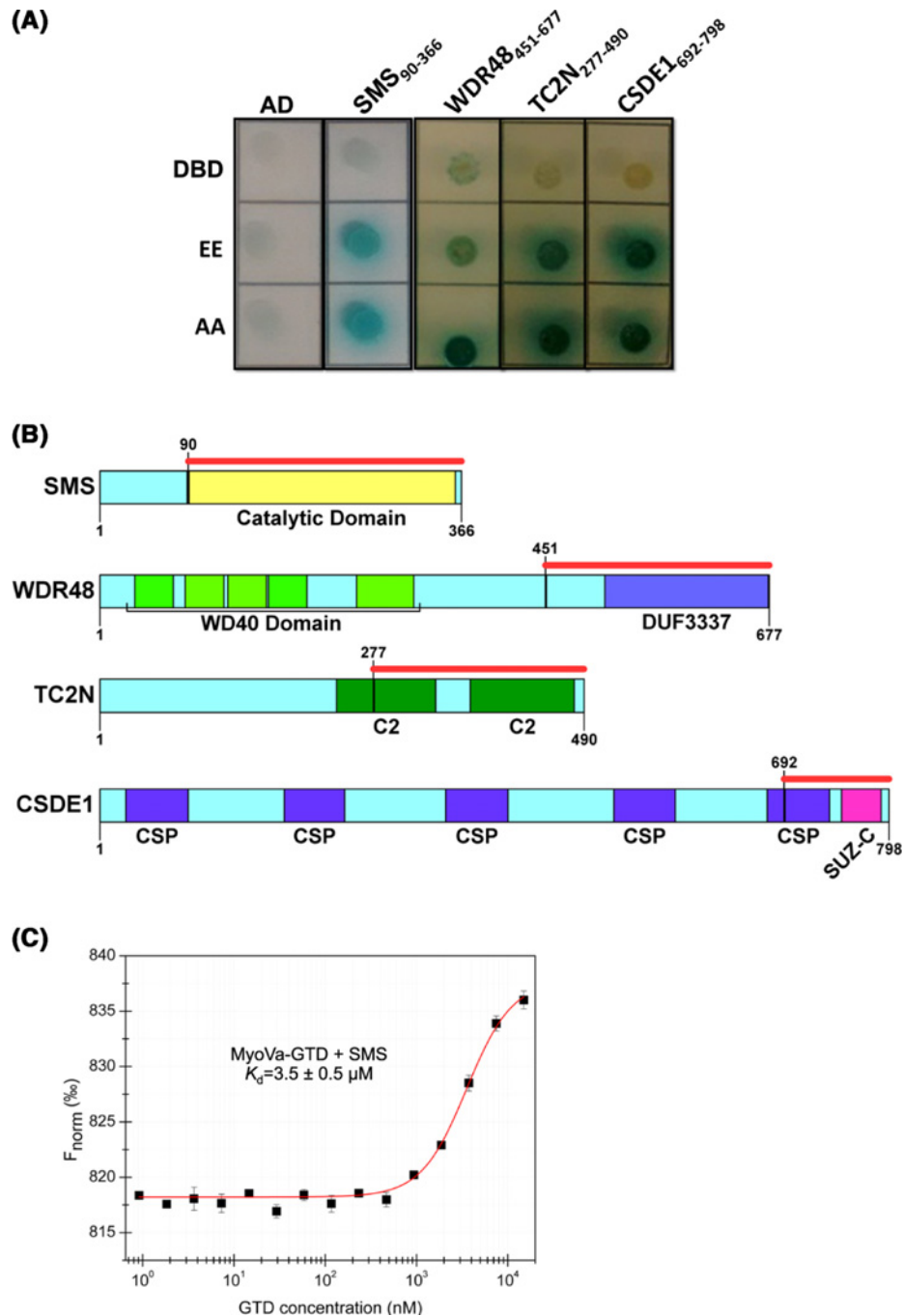


Figure 1. Yeast two-hybrid and *in vitro* assays reveal SMS as a novel binding partner of MyoVa-GTD

(A) Pairwise two-hybrid assays showing the activation of four reporter genes (QDO/X/A selective medium) in yeast cells co-transformed with pGADT7-prey (or empty pGADT7 as a control) plasmids and pGBKT7-GTD constructs (EE = phosphomimetic and AA = non-phosphorylated) showing that the identified interactions are not specific to the phosphomimetic mutant. The first line represents the negative control assays, where each clone was tested against the empty pGBKT7 vector (DBD). (B) Schematic representation of the domain architecture of the new-found partners. The red bar indicates the prey boundaries found in the yeast two-hybrid screening: SMS^{90–366} = catalytic domain of SMS (NCBI accession number: EAW98985); WDR48^{451–677} = DUF3337 domain of the WDR48 (NCBI accession number EAW64548); TC2N^{277–490} = contains the second C2 domain of the tandem C2 domains nuclear protein (TC2N; NCBI accession number: EAW81464); CSDE1^{692–798} = contains the SUZ-C domain of the cold shock domain-containing protein E1, isoform 4 (CSDE1; NCBI accession number: NP_001007554). Figures were made using SMART [19] and IBS [41]. (C) MST assays showing that MyoVa-GTD binds to SMS with a K_d in the low micromolar range. F_{norm} = normalized fluorescence. Data are presented as mean \pm SD (error bars) from triplicates.

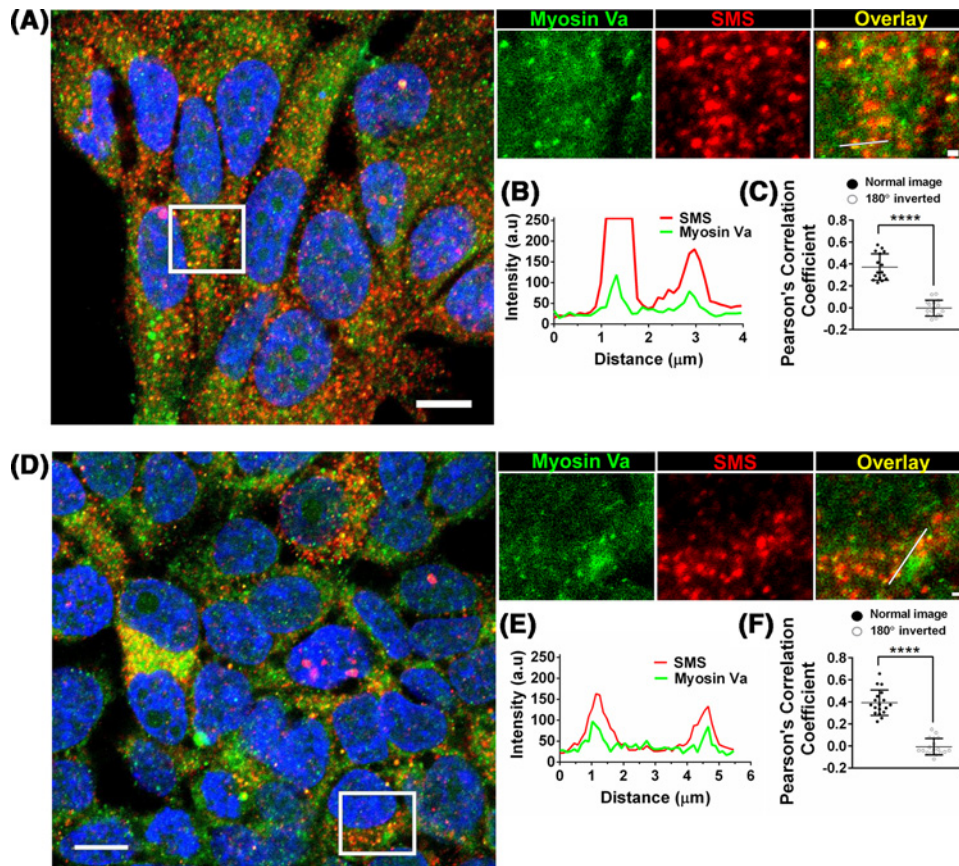


Figure 2. MyoVa and SMS localize together in discrete puncta at the cytoplasm

Immunocytochemistry showing the colocalization of MyoVa (green; anti-MyoVa-Medial tail) and SMS (red) labeling in MCF-7 (A-C) and SH-SY5Y (D-F) cell lines. The overlap of the fluorescent signals is shown in yellow (overlay). (B,E) Linescan analysis of two representative colocalization sites. (C, F) Pearson's correlation coefficients support the partial colocalization of MyoVa (green) and SMS (red) labeling. The correlation is based on the average of 16 and 18 independent cells, for MCF-7 and SH-SY5Y cells, respectively, with standard deviations shown. The correlation between MyoVa (rotated 180°) and SMS channels was used as negative control (random colocalization). Nucleus were stained with DAPI (Blue). Scale bar: 10 μm (field), 1 μm (zoom). **** $P \leq 0.001$ from two-tailed Wilcoxon's non-parametric rank test in C (because one of the populations were not normally distributed) and two-tailed paired *t* test in F).

According to qPCR analyses, the mRNA expression levels of SMS decreased upon *MYO5A*-silencing (Figure 3B,C), which correlated with a slight decrease in SMS protein content assessed by Western blot (Supplementary Figure S4). To investigate a possible correlation between depletion of MyoVa protein and SMS transcription, we also evaluated the expression of SMS in *MYO5A*-null primary fibroblasts isolated from patients with Griscelli Syndrome Type 1/Elejalde syndrome. As expected, the SMS expression was lower in cells lacking functional MyoVa compared with normal primary fibroblasts, indicating a role for MyoVa in the synthesis or stability of SMS mRNA (Figure 3D). In contrast, when the expression of *MYO5A* was stimulated upon neuron differentiation, the expression level of SMS also increased, further supporting a correlation between the expression of these two genes (Figure 3E-G).

Discussion

In this work, we reveal the direct interaction between MyoVa-GTD and four components of exosomes – WDR48, CSDE1, TC2N, and SMS – using a highly stringent yeast two-hybrid system. Furthermore, we validate the interaction between MyoVa-GTD and the enzyme SMS *in vitro*, and provide primary evidence about a new role for MyoVa in the expression and targeting of SMS into secretory vesicles.

MyoVa-GTD and SMS form complexes *in vitro* with a dissociation constant in the low micromolar range ($K_d = 3.5 \pm 0.5 \mu\text{M}$), which is typical of transient complexes and is similar to the affinity of MyoVa-GTD to other binding

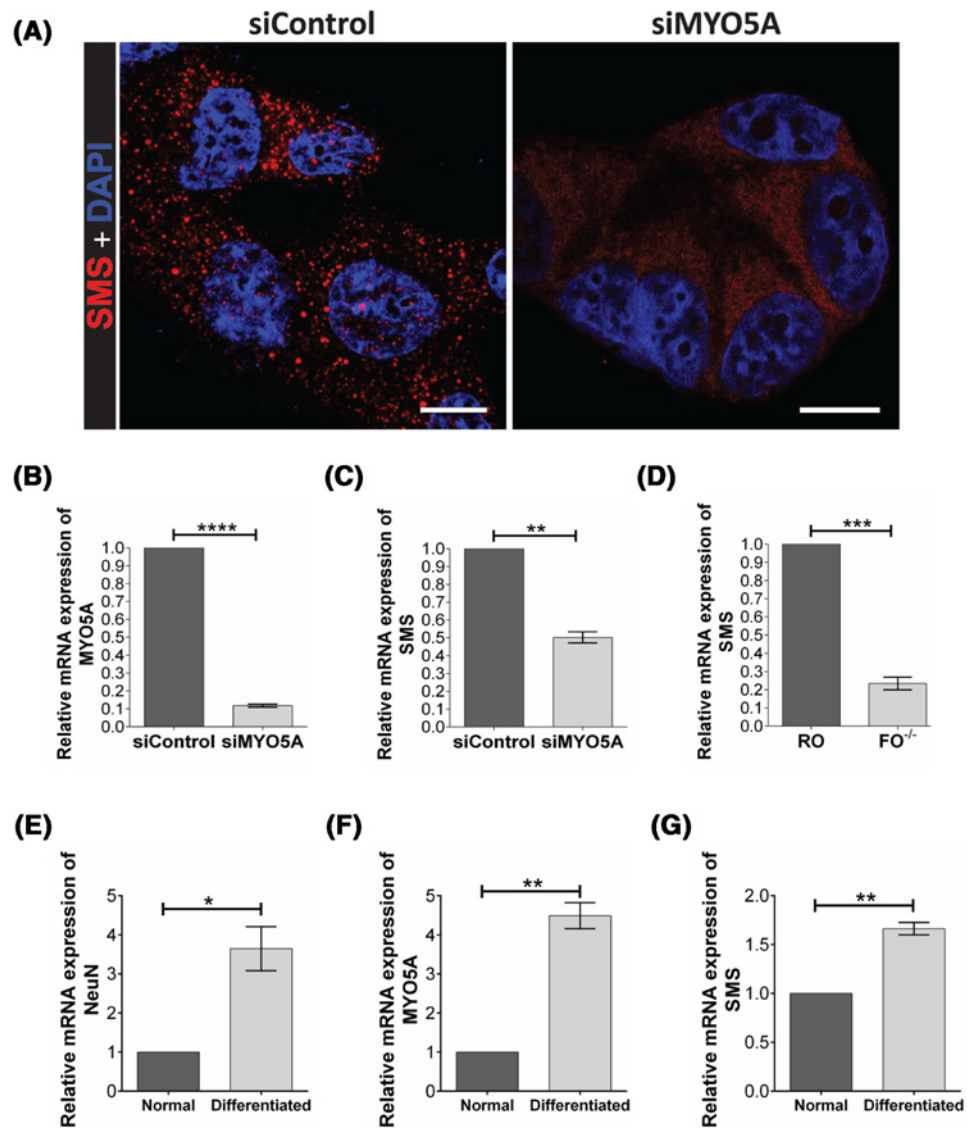


Figure 3. *MYO5A* knockdown affects SMS distribution and expression in MCF-7 cells

(A) Immunocytochemistry showing that the puncta distribution of SMS (siControl) became diffuse in cells treated with *siMYO5A*. Nucleus were stained with DAPI (Blue). Scale bar: 10 μ m. (B) qPCR showing that the *siMYO5A* treatment was effective to reduce *MYO5A* mRNA expression. (C) The qPCR showing the relative mRNA expression of *SMS* in cells treated with siControl or *siMYO5A* and in (D) *MYO5A*-null fibroblasts (FO^{-/-}) and the normal control (RO). The qPCR analysis of expression of the marker for neuronal differentiation *NeuN* (E), *MYO5A* (F), and *SMS* (G) in normal and differentiated neuronal SH-SY5Y cells. * $P \leq 0.05$; ** $P \leq 0.01$; *** $P \leq 0.001$, **** $P \leq 0.0001$. Paired *t* test, two-tailed.

partners, such as the C2 domains of RPGRIP1L (3–9 μ M, also determined by MST but using a covalent probe) [7]. The protein SMS has been found in the cytosol, in nuclear bodies and in exosomes [28–30]. This enzyme converts spermidine into spermine (EC 2.5.1.22) [31–33], a polyamine that acts as second messenger in neurotransmission, targeting receptors in postsynaptic membranes [34–36]. The vesicular storage of spermine and spermidine involves an active transporter from the SLC18 family, but the mechanisms coupling spermine synthesis to secretion are still elusive [37]. In this context, and based on our results showing the physical interaction between MyoVa-GTD and SMS, the colocalization of SMS and MyoVa in a subset of cytoplasmic vesicles and the more diffuse distribution of SMS protein upon *MYO5A* gene silencing, it is tempting to hypothesize that the actin-based motor MyoVa targets the enzyme that produces spermine to secretory vesicles for spermine secretion via exocytosis [37,38], and/or SMS

release via exosomes [28,29]. Moreover, whether and how the interaction between MyoVa and SMS influence the spermine synthase activity should be further evaluated in future studies.

Besides our RNAi studies show lower levels of SMS mRNA upon *MYO5A* silencing, other evidences support a correlation between *MYO5A* and SMS expression. In *MYO5A*-null fibroblasts, SMS transcripts are less abundant than in normal cells, indicating that functional MyoVa is required for the usual expression of SMS gene. Moreover, *MYO5A* and SMS are up-regulated in differentiated neurons and the proteins they encode are less abundant in human brains with Huntington's disease, a progressive neurodegenerative disorder [39]. Phenotypic traits further support a correlation between MyoVa and SMS, since patients harboring loss-of-function mutations in SMS or *MYO5A* genes share some neurological symptoms, including intellectual disability, seizures, and hypotonia [12,27,40].

In summary, the new interaction between MyoVa and exosomes components, including the enzyme SMS, and the co-occurrence of MyoVa and SMS in cytoplasmic vesicles bring new perspectives about the roles of this molecular motor in exocytic pathways, especially in the filling of exosomes and secretion of the neuromodulator spermine.

Availability of materials and data

Materials, data, and associated protocols will be promptly available to readers without undue qualifications in material transfer agreements.

Acknowledgements

The authors are grateful to Professor Jörg Kobarg for the assistance with the two-hybrid screen, to the Spectroscopy and Calorimetry Lab from LNBio, and to Dr. Fernanda A.H. Batista, Silmara Banzi Reis, Benedita de Souza, and Eduardo Tozatto for the technical assistance. The authors also thank the Multiuser Laboratories on Confocal the Department of Cell and Molecular Biology, Faculty of Medicine of Ribeirão Preto, USP, and the LaCTAD-UNICAMP.

Author contribution

Molecular cloning (L.G.D., L.H.P.A., and A.F.Z.N.); yeast two-hybrid (L.G.D. and L.H.P.A.); protein expression and purification (L.G.D. and A.F.Z.N.); microscale thermophoresis (L.G.D.); cell culture, siRNA knockdown, qPCR, and immunocytochemistry (R.M.P.S.J., L.G.D., and J.S.A.); fibroblasts assays (I.P.M. and E.M.E.); conception and design (L.G.D., R.M.P.S.J., E.M.E., P.O.G., and M.T.M.); data analysis and interpretation (L.G.D., R.M.P.S.J., P.O.G., E.M.E., L.H.P.A., and M.T.M.); manuscript writing (L.G.D., P.O.G., and M.T.M.); figures preparation (L.G.D., R.M.P.S.J., and P.O.G.) and manuscript revision (all authors).

Competing interests

The authors declare that there are no competing interests associated with the manuscript.

Funding

The present work was supported by FAPESP [grant number: 2014/09720-9 (to M.T.M.); grant numbers: 2018/04017-9 and 2013/08135-2 (to E.M.E.); grant number: 2014/00584-5 (to L.G.D.); grant number: 2011/20229-7 (to L.H.P.A.); grant number: 2009/14257-8 (to A.F.Z.N.); grant number: 2016/10862-8 (to J.S.A.); grant number: 2014/03989-6 (to R.M.P.S.J.)]. Grant to multiuser facilities [grant number: 2004/08868-0]; CNPq [grants numbers: 478059/2009-4 and 486841/2012-0 (to M.T.M.), grants numbers: 457603/2013-5 and 309187/2015-0 (to E.M.E.)] and CAPES [grant number: 88887.137811/2017-00 (to R.M.P.S.J.)].

Abbreviations

AD, activation domain; DBD, DNA-binding domain; DMEM, Dulbecco's modified Eagle's medium; GTD, globular tail domain; MST, microscale thermophoresis; MyoVa, myosin Va; NTA, nitrilotriacetic acid; ORF, open reading frame; qPCR, quantitative PCR; SEC, size-exclusion chromatography; SMS, spermine synthase; TEV, tobacco etch virus.

References

- 1 Hammer, 3rd, J.A. and Wagner, W. (2013) Functions of class V myosins in neurons. *J. Biol. Chem.* **288**, 28428–28434, <https://doi.org/10.1074/jbc.R113.514497>
- 2 Rudolf, R., Bittins, C.M. and Gerdes, H.H. (2011) The role of myosin V in exocytosis and synaptic plasticity. *J. Neurochem.* **116**, 177–191, <https://doi.org/10.1111/j.1471-4159.2010.07110.x>
- 3 Trybus, K.M. (2008) Myosin V from head to tail. *Cell. Mol. Life Sci.* **65**, 1378–1389, <https://doi.org/10.1007/s00018-008-7507-6>
- 4 Brozzi, F. et al. (2012) Molecular mechanism of myosin Va recruitment to dense core secretory granules. *Traffic* **13**, 54–69, <https://doi.org/10.1111/j.1600-0854.2011.01301.x>
- 5 Sonal et al. (2014) Myosin Vb mediated plasma membrane homeostasis regulates peridermal cell size and maintains tissue homeostasis in the zebrafish epidermis. *PLoS Genet.* **10**, e1004614, <https://doi.org/10.1371/journal.pgen.1004614>

- 6 Sladewski, T.E., Kremntsova, E.B. and Trybus, K.M. (2016) Myosin Vc is specialized for transport on a secretory superhighway. *Curr. Biol.* **26**, 2202–2207, <https://doi.org/10.1016/j.cub.2016.06.029>
- 7 Assis, L.H. et al. (2017) The molecular motor Myosin Va interacts with the cilia-centrosomal protein RPGRIP1L. *Sci. Rep.* **7**, 43692, <https://doi.org/10.1038/srep43692>
- 8 Wei, Z. et al. (2013) Structural basis of cargo recognitions for class V myosins. *Proc. Natl. Acad. Sci. U.S.A.* **110**, 11314–11319, <https://doi.org/10.1073/pnas.1306768110>
- 9 Nascimento, A.F. et al. (2013) Structural insights into functional overlapping and differentiation among myosin V motors. *J. Biol. Chem.*, <https://doi.org/10.1074/jbc.M113.507202>
- 10 Pylypenko, O. et al. (2013) Structural basis of myosin V Rab GTPase-dependent cargo recognition. *Proc. Natl. Acad. Sci. U.S.A.* **110**, 20443–20448, <https://doi.org/10.1073/pnas.1314329110>
- 11 Elejalde, B.R. et al. (1979) Mutations affecting pigmentation in man: I. Neuroectodermal melanolyosomal disease. *Am. J. Med. Genet.* **3**, 65–80, <https://doi.org/10.1002/ajmg.1320030112>
- 12 Pastural, E. et al. (1997) Griscelli disease maps to chromosome 15q21 and is associated with mutations in the myosin-Va gene. *Nat. Genet.* **16**, 289–292, <https://doi.org/10.1038/ng0797-289>
- 13 Provance, D.W., James, T.L. and Mercer, J.A. (2002) Melanophilin, the product of the leaden locus, is required for targeting of myosin-Va to melanosomes. *Traffic* **3**, 124–132, <https://doi.org/10.1034/j.1600-0854.2002.030205.x>
- 14 Schiaffino, M.V. (2010) Signaling pathways in melanosome biogenesis and pathology. *Int. J. Biochem. Cell Biol.* **42**, 1094–1104, <https://doi.org/10.1016/j.biocel.2010.03.023>
- 15 Landrock, K.K. et al. (2018) Pleiotropic neuropathological and biochemical alterations associated with Myo5a mutation in a rat Model. *Brain Res.* **1679**, 155–170, <https://doi.org/10.1016/j.brainres.2017.11.029>
- 16 Papadopoulos, A. et al. (2013) The cortical acto-Myosin network: from diffusion barrier to functional gateway in the transport of neurosecretory vesicles to the plasma membrane. *Front. Endocrinol.* **4**, 153, <https://doi.org/10.3389/fendo.2013.00153>
- 17 Mathivanan, S. et al. (2012) ExoCarta 2012: database of exosomal proteins, RNA and lipids. *Nucleic. Acids Res.* **40**, D1241–D1244, <https://doi.org/10.1093/nar/gkr828>
- 18 Altschul, S.F. et al. (1990) Basic local alignment search tool. *J. Mol. Biol.* **215**, 403–410, [https://doi.org/10.1016/S0022-2836\(05\)80360-2](https://doi.org/10.1016/S0022-2836(05)80360-2)
- 19 Schultz, J. et al. (1998) SMART, a simple modular architecture research tool: Identification of signaling domains. *Proc. Natl. Acad. Sci. U.S.A.* **95**, 5857–5864
- 20 Bertani, G. (1951) Studies on lysogeny I.: the mode of phage liberation by lysogenic *Escherichia coli*. *J. Bacteriol.* **62**, 293–300
- 21 Kapust, R.B. et al. (2001) Tobacco etch virus protease: mechanism of autolysis and rational design of stable mutants with wild-type catalytic proficiency. *Protein. Eng.* **14**, 993–1000, <https://doi.org/10.1093/protein/14.12.993>
- 22 Lagache, T. et al. (2015) Statistical analysis of molecule colocalization in bioimaging. *Cytometry A* **87**, 568–579, <https://doi.org/10.1002/cyto.a.22629>
- 23 Livak, K.J. and Schmittgen, T.D. (2001) Analysis of relative gene expression data using real-time quantitative PCR and the 2⁻(Delta Delta C(T)) Method. *Methods* **25**, 402–408, <https://doi.org/10.1006/meth.2001.1262>
- 24 Encinas, M. et al. (2000) Sequential treatment of SH-SY5Y cells with retinoic acid and brain-derived neurotrophic factor gives rise to fully differentiated, neurotrophic factor-dependent, human neuron-like cells. *J. Neurochem.* **75**, 991–1003, <https://doi.org/10.1046/j.1471-4159.2000.0750991.x>
- 25 Bruckner, A. et al. (2009) Yeast two-hybrid, a powerful tool for systems biology. *Int. J. Mol. Sci.* **10**, 2763–2788, <https://doi.org/10.3390/ijms10062763>
- 26 Kesler, S.R. et al. (2009) The impact of spermine synthase (SMS) mutations on brain morphology. *Neurogenetics* **10**, 299–305, <https://doi.org/10.1007/s10048-009-0184-2>
- 27 Cason, A.L. et al. (2003) X-linked spermine synthase gene (SMS) defect: the first polyamine deficiency syndrome. *Eur. J. Hum. Genet.* **11**, 937–944, <https://doi.org/10.1038/sj.ejhg.5201072>
- 28 Overbye, A. et al. (2015) Identification of prostate cancer biomarkers in urinary exosomes. *Oncotarget* **6**, 30357–30376, <https://doi.org/10.18632/oncotarget.4851>
- 29 Rouillard, A.D. et al. (2016) The harmonizome: a collection of processed datasets gathered to serve and mine knowledge about genes and proteins. *Database* **2016**, <https://doi.org/10.1093/database/baw100>
- 30 Thul, P.J. et al. (2017) A subcellular map of the human proteome. *Science* **356**, <https://doi.org/10.1126/science.aal3321>
- 31 Hibasami, H. et al. (1980) Studies of inhibition of rat spermidine synthase and spermine synthase. *Biochem. J.* **187**, 419–428, <https://doi.org/10.1042/bj1870419>
- 32 Pajula, R.L., Raina, A. and Eloranta, T. (1979) Polyamine synthesis in mammalian tissues. Isolation and characterization of spermine synthase from bovine brain. *Eur. J. Biochem.* **101**, 619–626, <https://doi.org/10.1111/j.1432-1033.1979.tb19756.x>
- 33 Wu, H. et al. (2008) Crystal structure of human spermine synthase: implications of substrate binding and catalytic mechanism. *J. Biol. Chem.* **283**, 16135–16146, <https://doi.org/10.1074/jbc.M710323200>
- 34 Casero, Jr, R.A. and Marton, L.J. (2007) Targeting polyamine metabolism and function in cancer and other hyperproliferative diseases. *Nat. Rev. Drug Discov.* **6**, 373–390, <https://doi.org/10.1038/nrd2243>
- 35 Williams, K. (1997) Modulation and block of ion channels: a new biology of polyamines. *Cell. Signal.* **9**, 1–13, [https://doi.org/10.1016/S0898-6568\(96\)00089-7](https://doi.org/10.1016/S0898-6568(96)00089-7)
- 36 Ogden, K.K and Traynelis, S.F. (2011) New advances in NMDA receptor pharmacology. *Trends Pharmacol. Sci.* **32**, 726–733, <https://doi.org/10.1016/j.tips.2011.08.003>
- 37 Hiasa, M. et al. (2014) Identification of a mammalian vesicular polyamine transporter. *Sci. Rep.* **4**, 6836, <https://doi.org/10.1038/srep06836>

- 38 Masuko, T. et al. (2003) Polyamine transport, accumulation, and release in brain. *J. Neurochem.* **84**, 610–617, <https://doi.org/10.1046/j.1471-4159.2003.01558.x>
- 39 Ratovitski, T. et al. (2016) Quantitative proteomic analysis reveals similarities between Huntington's disease (HD) and Huntington's disease-like 2 (HDL2) human brains. *J. Proteome Res.* **15**, 3266–3283, <https://doi.org/10.1021/acs.jproteome.6b00448>
- 40 Becerra-Solano, L.E. et al. (2009) A missense mutation, p.V132G, in the X-linked spermine synthase gene (SMS) causes Snyder-Robinson syndrome. *Am. J. Med. Genet. A* **149a**, 328–335, <https://doi.org/10.1002/ajmg.a.32641>
- 41 Liu, W. et al. (2015) IBS: an illustrator for the presentation and visualization of biological sequences. *Bioinformatics* **31**, 3359–3361, <https://doi.org/10.1093/bioinformatics/btv362>
- 42 Yin, J. et al. (2015) Structural insights into WD-repeat 48 activation of ubiquitin-specific protease 46. *Structure* **23**, 2043–2054, <https://doi.org/10.1016/j.str.2015.08.010>
- 43 Hunt, S.L. et al. (1999) UNR, a cellular cytoplasmic RNA-binding protein with five cold-shock domains, is required for internal initiation of translation of human rhinovirus RNA. *Genes Dev.* **13**, 437–448, <https://doi.org/10.1101/gad.13.4.437>
- 44 Kalra, H. et al. (2012) Vesiclepedia: a compendium for extracellular vesicles with continuous community annotation. *PLoS Biol.* **10**, e1001450, <https://doi.org/10.1371/journal.pbio.1001450>